Experiments in Fluids 24 (1998) 416–423 © Springer-Verlag 1998

A four-sensor hot-wire probe system for three-component velocity measurement

K. S. Wittmer, W. J. Devenport, J. S. Zsoldos

Abstract A velocity measurement system based on a miniature four-sensor hot-wire probe capable of simultaneous three-component measurements throughout a wide range of flow angles has been developed. The calibration technique allows measurements to be made throughout the acceptance cone of the probe without being restricted by the errors associated with analytic angle response equations. This technique is based upon look-up tables with values which tend to vary slowly, allowing a simple interpolation scheme to be used. Measurements made in a turbulent pipe flow verify the accuracy of the technique.

1 Introduction

Multiple sensor hot-wire probes offer some desirable characteristics for measuring moderately turbulent flows away from walls. They give continuous, low-noise signals required for the measurement of low turbulence levels and velocity spectra; and can provide the type of statistical turbulence information usually used by turbulence modellers. X-wire probes are relatively easy to operate but produce large uncertainties in the complete Reynolds stress tensor field because all three velocity components cannot be measured simultaneously. Triple wire probes are capable of simultaneous three-component measurements, but their typical sensor configuration make them sensitive to velocity gradient errors, particularly those associated with streamwise vorticity (Devenport et al. 1992). Four-sensor probes consisting of two orthogonal X-wire arrays (Fig. 1) – normally associated with vorticity measurements (Kovasznay 1954) – are capable of simultaneous three-component velocity measurements from a relatively compact measurement volume and appear to overcome some of the gradient error problems associated with triple wire probes.

Received: *27 September 1996/Accepted*: *20 October 1997*

K. S. Wittmer, W. J. Devenport, J. S. Zsoldos
Virginia Tech Department of Aerospace and Ocean Engineering 215 Randolph Hall, Blacksburg, Virginia 24061-0203, USA

Correspondence to: W. J. Devenport

The authors would like to acknowledge the support over many years of NASA, (in particular Drs. Tom Brooks, Casey Burley, and Mike Marcolini), ONR (in particular Dr. L. Patrick Purtell), and DARPA (in particular Mr. Gary Jones) under which this measurement system was developed and refined. Grant numbers were NASA: NAG-1-1119 and NAG-1-1539, ONR: N00014-92-J-4087 and N00014-91-J-1773.

Initially it might appear that there are several difficulties associated with the use of a four-sensor probe for velocity measurements. Standard hot-wire angle response equations derived via Jorgensen's method (Jorgensen 1971) yield a non-linear set of equations which are inaccurate at large flow angles due to effects such as prong interference. Most direct calibration methods improve accuracy but usually require sophisticated interpolation schemes. The calibration technique for the four-sensor probe described here overcomes these limitations. The complete hot-wire system is capable of rapid and accurate, three-component, velocity, turbulence, and spectral measurements.

2 Four-sensor probes and measurement system

Probes were manufactured by Auspex Corporation (type AVOP-4-100). Eight stainless steel or nickel plated tungsten tapered prongs (75 μm in diameter at their tips) position the wires some 40 mm upstream of the main part of the probe (Fig. 2) inside a measurement volume of approximately 0.5 mm^3. The sensors are etched tungsten wire of 5 μm diameter with an approximate length of 0.8 mm giving a length to diameter ratio of about 160. Sensors are arranged as two orthogonal X-wire arrays with each wire inclined at a nominal 45° angle to the probe axis. Figure 1 defines the coordinate

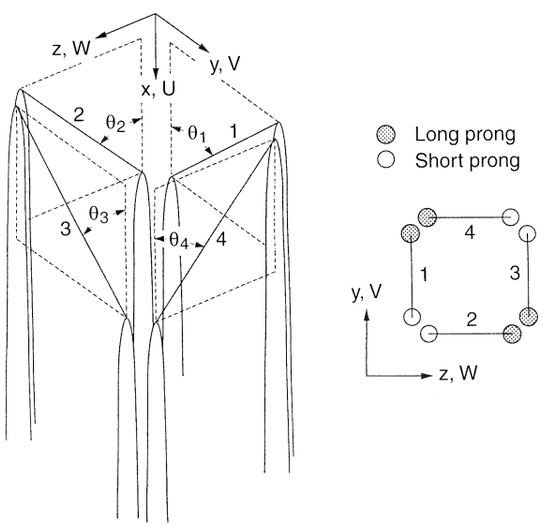

Fig. 1. Four-sensor probe prong geometry

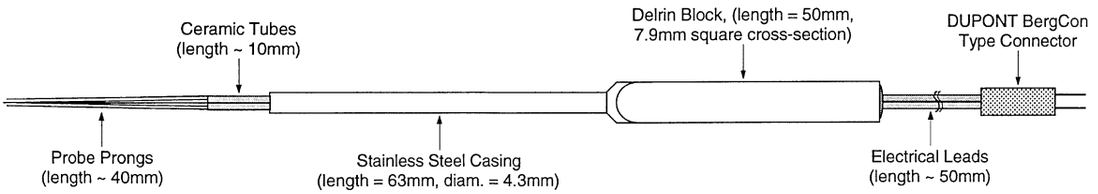

Fig. 2. Auspex Corporation four-sensor probe (type AVOP-4-100) construction

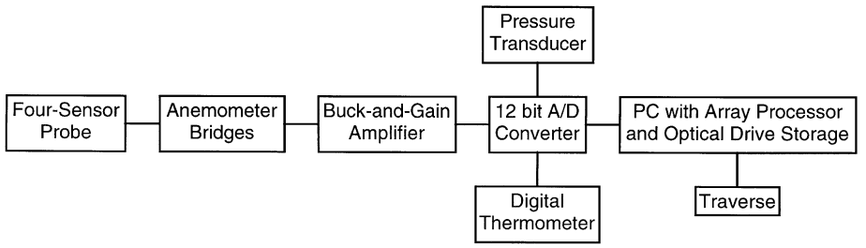

Fig. 3. Measurement system block diagram

system and sensor numbering convention. The probe aligned velocity components U, V and W are directed along the x, y and z axes respectively. One X-wire array is formed by sensors 1 and 3 (both parallel to the x–y plane), the other X-wire array is formed by sensors 2 and 4 (both parallel to the x–z plane). The subscript i is used to denote quantities associated with the i-th sensor where $i = 1 \ldots 4$. Angles (θ_i) associated with the sensors are acute angles measured from the x-axis.

A block diagram of the measurement system is shown in Fig. 3. Hot-wire sensors are operated separately using Dantec 56C17/56C01 constant temperature anemometer units. The anemometer bridges are optimized to give a frequency response greater than 25 kHz. Output voltages from the bridges are recorded by an IBM AT compatible computer using an Analogic 12 bit HSDAS-12 A/D converter which contains four separate converters. Hot-wire signals are buffered by four $\times 10$ buck-and-gain amplifiers. The amplifiers contain calibrated RC-filters which limit their frequency response to 50 kHz, providing high-frequency noise attenuation. The buck-and-gain is used so that the anemometer voltage outputs span the full range of the A/D converter over the velocity range of the measurement. Voltage outputs from a digital thermometer and pressure transducer are also sampled by the A/D converter. The digitized raw voltage data is stored on optical disk. An 18-8 Laboratories PL2510 array processor is used to calculate velocity estimates "on line". Calibration procedures outside of the wind tunnel are accomplished by placing the probe in the uniform potential jet of a TSI model 1125 calibrator. The probe can be manually pitched and yawed to a known angle in this jet with the use of two rotary stages.

3
Calibration technique

Calibration of a multiple sensor hot-wire probe is in essence the determination of an empirical relationship between the output voltages of the sensors and the components of the velocity vector. Determining this three-dimensional function purely by measurement is, in many circumstances, a prohibitively time-consuming task considering the frequent recalibration that must be performed to account for fouling and aging of the sensors. One therefore seeks a simplification of this function to a manageable level without significantly compromising the accuracy of the results.

The central assumption of the present scheme is that the calibration can be split into two components. First, a traditional King's law type calibration between sensor voltage and an effective cooling velocity that accounts for the wire properties and may be frequently repeated to account for their drift due to fouling and aging.[1] Second, a relatively sophisticated angle calibration between the four effective velocities and the three-components that accounts for sensor and prong geometry effects that requires only occasional repetition. Our calibration technique is inspired by the method of Mathioudakis and Breugelmans (1985) which greatly extended the useful range of flow angles which can be accurately measured by a triple wire probe.

3.1
Angle calibration

The purpose of the angle calibration is to establish the relationship

$$\mathbf{V} = U\hat{i} + V\hat{j} + W\hat{k} = \mathbf{f}(U_{\mathrm{eff}_1}, U_{\mathrm{eff}_2}, U_{\mathrm{eff}_3}, U_{\mathrm{eff}_4}) \quad (1)$$

through measurement of a specific set of points and interpolation between those points. Here $\mathbf{V}$ is the (instantaneous) velocity vector and U_{eff_i} are the effective velocities inferred from the King's law calibration (below). To maximize the accuracy of the calibration and minimize the number of measurements required to establish it, it is desirable to cast

[1] The bridge output voltages are corrected for small changes in ambient temperature using the method of Bearman (1971).

f in a form in which the interpolation is carried out only on quantities that vary slowly. We have chosen

$$V = f_1(V_e/Q_e,\ W_e/Q_e)\cdot Q_e + V_e \tag{2}$$

$$W = f_2(V_e/Q_e,\ W_e/Q_e)\cdot Q_e + W_e \tag{3}$$

$$Q = f_3(V_e/Q_e,\ W_e/Q_e)\cdot Q_e + Q_e \tag{4}$$

where Q is the magnitude of the velocity vector. Obviously $U = \sqrt{Q^2 - V^2 - W^2}$. The new variables V_e, W_e, Q_e are rough estimates of the velocity components and vector magnitude obtained from the effective velocities using approximate analytic functions so that the functions f_1, f_2, f_3 contain all the implicit interpolation. By writing the calibration in this form, we gain control over task facing the interpolation scheme — the better the analytic functions used to obtain V_e, W_e, Q_e, the smaller the variations in f_1, f_2, f_3 that must be interpolated, and the less the significance of the interpolated part. Note that we have assumed that these functions are independent of the velocity magnitude (i.e. Reynolds number). This is not absolutely necessary but was found to be a very good approximation, as is demonstrated below.

In the present work we obtained the analytic functions for V_e, W_e, and Q_e simply by assuming that the sensors respond only to the velocity component normal to them. This choice is not necessarily optimum – there are obviously more sophisticated analytic approximations to the response of a hot-wire – but it was found to be perfectly adequate for the present purpose of yielding functions f_1, f_2, f_3 suitable for simple interpolation. Using the geometry (in particular the wire angles θ_i) and coordinate system of Fig. 1 we write

$$U^2_{\mathrm{eff}_1} = (U_e \sin\theta_1 + V_e \cos\theta_1)^2 + W_e^2 \tag{5}$$

$$U^2_{\mathrm{eff}_2} = (U_e \sin\theta_2 + W_e \cos\theta_2)^2 + V_e^2 \tag{6}$$

$$U^2_{\mathrm{eff}_3} = (U_e \sin\theta_3 - V_e \cos\theta_3)^2 + W_e^2 \tag{7}$$

$$U^2_{\mathrm{eff}_4} = (U_e \sin\theta_4 - W_e \cos\theta_4)^2 + V_e^2 \tag{8}$$

Assuming V_e^2/U_e^2 and W_e^2/U_e^2 terms are negligible compared to 1 or $U_e V_e/U_e^2$ and $\sqrt{1+x}$ may be approximated as $1+\frac{1}{2}x$ for $x \ll 1$, Eqs. (5)–(8) can be linearized to yield

$$V_e = \frac{C_1\sqrt{C_3}U_{\mathrm{eff}_3} - C_3\sqrt{C_1}U_{\mathrm{eff}_1}}{C_1 D_3 - C_3 D_1} \tag{9}$$

$$W_e = \frac{C_2\sqrt{C_4}U_{\mathrm{eff}_4} - C_4\sqrt{C_2}U_{\mathrm{eff}_2}}{C_2 D_4 - C_4 D_2} \tag{10}$$

$$U_e = \frac{1}{2}\left(\frac{U_{\mathrm{eff}_1}}{\sqrt{C_1}} - \frac{D_1}{C_1}V_e + \frac{U_{\mathrm{eff}_2}}{\sqrt{C_2}} - \frac{D_2}{C_2}W_e\right) \tag{11}$$

where $C_i = \sin^2\theta_i$ and $D_i = \sin\theta_i \cos\theta_i$. Note that we have averaged the two U_e relations obtained from Eqs. (5) and (7), and (6) and (8), to minimize gradient errors resulting from axial vorticity (see Appendix).

Sensor angles were determined both by direct measurement (with the use of a tool-makers microscope) and by measuring the ratio between the effective velocity with the sensor normal to the flow and the probe axis aligned with the flow. The results were in all cases nearly identical, but varied by as much as 5° from the nominal sensor angle of 45°.

To determine the functions f_1, f_2, f_3, the probe was placed in the jet of the TSI calibrator to measure the cooling velocities as the probe is pitched and yawed over all likely angle combinations; usually $\pm 45°$ in increments of 5° or less. At each angle, velocity component estimates are compared with the actual velocity components U, V, W inferred from the known flow angles to determine f_1, f_2, f_3 from Eqs. (2)–(4).

To ensure that f_1, f_2, f_3 are single valued functions, points outside the acceptance cone of the probe must be eliminated. The acceptance cone is the region within which there is a single valued mapping between $(V_e/Q_e,\ W_e/Q_e)$ and $(V/Q,\ W/Q)$. The edge of the acceptance cone may therefore be identified by a change in sign of the Jacobian

$$\frac{\partial(V_e/Q_e,\ W_e/Q_e)}{\partial(V/Q,\ W/Q)}$$

which is easily computed numerically from the calibration data.

Figure 4 shows the acceptance cone of a typical probe and the angle calibration points within it used to determine f_1, f_2, f_3. The acceptance cone has a roughly diamond shaped limit indicating that larger flow angles can be measured if the flow direction corresponds to a near pure pitch (θ_z) or yaw (θ_y) (refer to Fig. 1 for coordinate system). The limit corresponds approximately to the angle at which reverse flow occurs on a sensor. The maximum flow angle which can be measured in pure pitch or yaw for this particular probe is approximately 40°. However, regardless of the roll orientation of the probe, flow angles less than 30° can always be measured. Contours of f_1, f_2, f_3 are shown in Fig. 5 for flow angles within the acceptance cone. These plots show that sophisticated interpolation is not required because f_1, f_2, f_3 vary slowly over most of the acceptance cone — an advantage of this method over others in which look up tables are used (e.g. Browne et al. 1989,

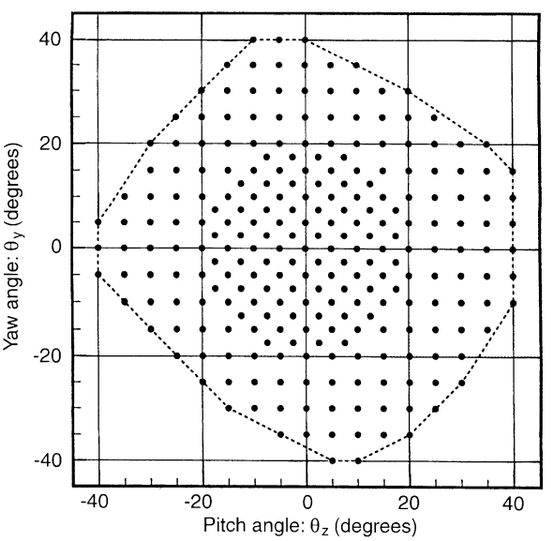

Fig. 4. Angle calibration points within the acceptance cone (indicated by dashed line) used to determine f_1, f_2, f_3 with $Q = 25$ m/s

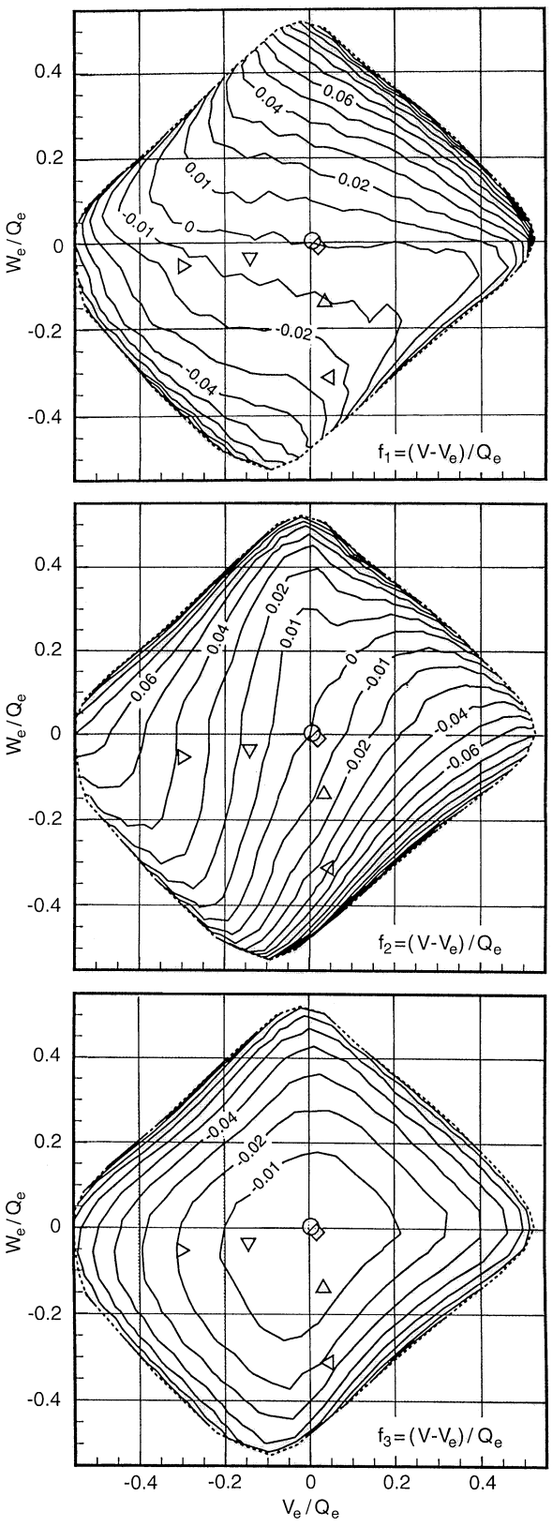

Fig. 5. Contours of f_1, f_2, f_3 throughout acceptance cone of probe measured with $Q = 25$ m/s. Symbols represent locations within the acceptance cone of the mean flow for the pipe flow measurements and are consistent with the legends in Figs. 7–9

Leuptow et al. 1988, Döbbeling et al. 1990). Contours of f_1 indicate that the V-component of velocity is estimated well from Eq. (9) if the probe is in pure yaw, and likewise, contours of f_2 indicate that the W-component of velocity is estimated well from Eq. (10) if the probe is in pure pitch. Contours of f_2 have an appearance similar to f_1 if rotated 90° – as expected due to the symmetry of the sensors. Away from pure pitch and yaw, however, the errors are significant and the interpolated functions are clearly needed for accurate measurement. The function f_3 shows that Q is consistently over-predicted by the linearized equations, and the corrections vary even more slowly than f_1 and f_2.

To permit rapid application of the angle calibration, ordered look-up tables for f_1, f_2, f_3 were created by linearly interpolating the data using triangulation (linear interpolation in the plane defined by the three surrounding points). These tables, representing 32×32 evenly spaced values of V_e/Q_e, W_e/Q_e over the acceptance cone of the probe, were interpolated using a bi-linear interpolation scheme when applying the calibration to measurements.

To examine the combined effects of the triangulation and bi-linear interpolation procedures and to verify the calibration and measurement reduction software, velocity measurements obtained from an angle calibration were reprocessed using the angle calibration and compared to those inferred from the pitch and yaw angle of the probe. Residual errors were typically less than $0.05\%Q$ over the acceptance cone.

A major advantage of this direct angle calibration method is that accurate measurements can be made for non-ideal probe geometries. For example, a probe whose sensors do not lie precisely in the x–y and y–z planes (see Fig. 1) can be calibrated just as easily. Furthermore, we have found through repeated calibration of the probe over many years of application of this technique that the angle calibration is almost completely insensitive to sensor properties if the probe tip geometry remains unaltered. As a result it is only necessary to recalibrate occasionally over the life of the probe. The calibration is also relatively insensitive to Reynolds number, as is assumed in this formulation. This is illustrated in Fig. 6 where, for example, f_2 has been measured at jet velocities of 17.7 m/s and 12.5 m/s with the same probe represented in Fig. 5 where the jet speed was 25 m/s. Comparing all three speeds, differences of less than 1% exist even though the velocity magnitude varies by a factor of two. Similar invariance was observed for f_1 and f_3.

3.2 Velocity calibration

Velocity calibrations are performed for two purposes: (a) to provide the relationship between the four sensor output voltages (E_i) and the effective velocities needed to perform the angle calibration, and (b) to update that relationship to account for changes in the cooling properties of the sensors during prolonged wind tunnel measurements.

Prior to angle calibration, velocity calibrations are performed in the calibrator jet with the probe axis aligned with the flow direction. The sensor output voltages are correlated with the jet velocity using King's law

$$E_i^2 = A_i + B_i U_{\mathrm{eff}_i}^{0.45} \tag{12}$$

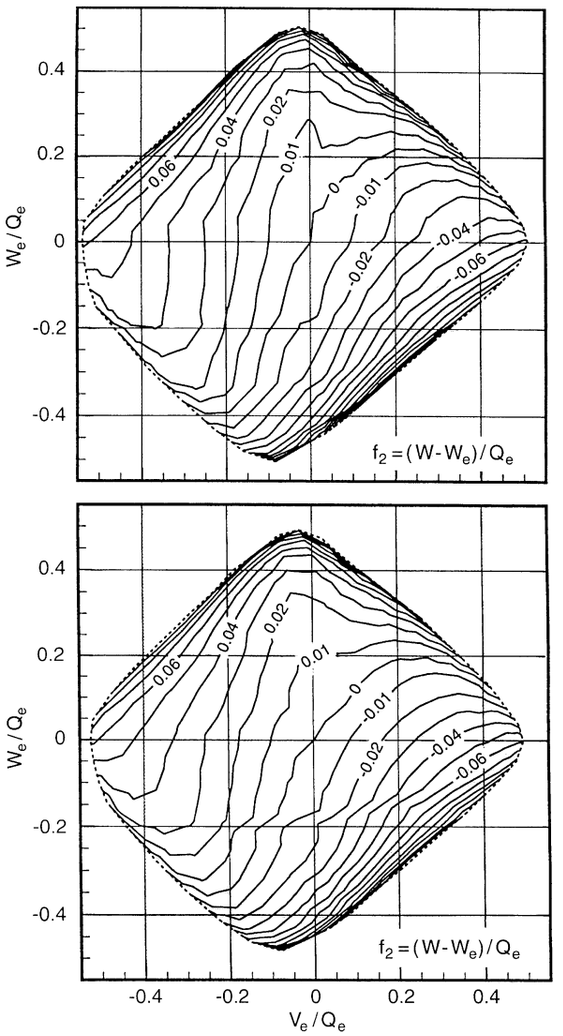

Fig. 6. Effects of Reynolds number on f_2. Top figure is for $Q=17.7$ m/s, bottom is for $Q=12.5$ m/s. Compare with Fig. 5 for $Q=25$ m/s

where U_{eff_i} is obtained from the jet velocity using the reduction of Eqs. (5)–(8) with $V=W=0$. This guarantees that the functions f_1, f_2, f_3 are zero for zero pitch and yaw.

Subsequent velocity calibrations can also be performed, if necessary, with a known misalignment between the probe axis and flow direction. The only difference is that the effective velocities are determined from the inversion of the angle calibration for the values of U, V, W calculated from the flow velocity and misalignment angle.[2] This method is particularly useful during extended wind tunnel measurements since it allows the probe to be calibrated in the free stream without performing a tedious alignment of the probe. To determine the misalignment angle in this circumstance we used a 7-hole yaw probe with a mount and angle calibration matched to that of the hot-wire probe.

[2]For small misalignement angles use of the look-up tables is not necessary and Eqs. (5)–(8) may be used since f_1, f_2, f_3 remain very close to zero for small angles as evidenced by Fig. 5.

Note that the velocity calibration procedure assumes implicitly that the angle calibration is independent of flow velocity, as demonstrated above.

4 Measurements and verification

To verify the accuracy of the hot-wire system and calibration techniques, measurements were made in a fully developed turbulent pipe flow. This flow has the useful property that the shear stress distribution can be determined from the pressure drop along the pipe. Specifically, the total axial-radial shear stress (τ_{xr}) varies linearly from 0 at the pipe centerline to a maximum of τ_w at the pipe wall. The wall shear is given by the pressure drop along the pipe as

$$\tau_w = \frac{R}{2}\frac{\mathrm{d}P}{\mathrm{d}x} \tag{13}$$

The shear stress in the flow is the sum of laminar and turbulent stresses i.e.

$$\tau = \mu\frac{\partial U_x}{\partial r} - \rho\overline{u_x u_r} \tag{14}$$

The turbulent shear stress can be explicitly determined by using the mean velocity profile to calculate the laminar stress. Following Nikuradse (1932), the mean axial flow velocity profile should be well represented by the $\frac{1}{7}$th-power law:

$$\frac{U_x}{U_0} = C\left(1-\frac{r}{R}\right)^{1/7} \tag{15}$$

for $1-r/R<0.9$ at a Reynolds number based on the average flow velocity through the pipe of 1×10^5 where U_0 is the mean velocity at the pipe centerline, R is the pipe radius, and C is a constant.

The pipe flow apparatus documented previously by Shaffer (1985) was used. The inside diameter of the pipe is 0.08 m and it has a length of approximately 240 diameters after flow conditioning honeycomb and screens. For the present measurements, the centerline velocity at the exit plane of the pipe was set of 25 m/s corresponding to a Reynolds number based upon the pipe diameter and average velocity of about 1×10^5. The pressure drop was measured along the last 75 diameters to calculate a friction velocity ($U_*=\sqrt{\tau_w/\rho}$ of 0.96 m/s.

All measurements were made at the exit plane of the pipe in radial profiles. Six orientations of the probe were used to test the ability of the probe to measure all three velocity components at various locations within the acceptance cone. Two sets of profile measurements were made with the axis of the probe roughly aligned with the axis of the pipe: the difference between the two being a roll angle of 90°. The probe was then pitched roughly 10° and measurements were made for roll angles of 0 and 90°. Likewise, the final two sets of measurements were made with the probe pitched at approximately 20°. The orientations of the probe relative to the mean flow direction are shown on the angle calibration plots of Fig. 5. Five of the six orientations are comfortably within the acceptance cone bounds. However, the case of 20° pitch, 0° roll ($\lhd$) is close to the edge of the acceptance cone due to the non-ideal geometry of the probe.

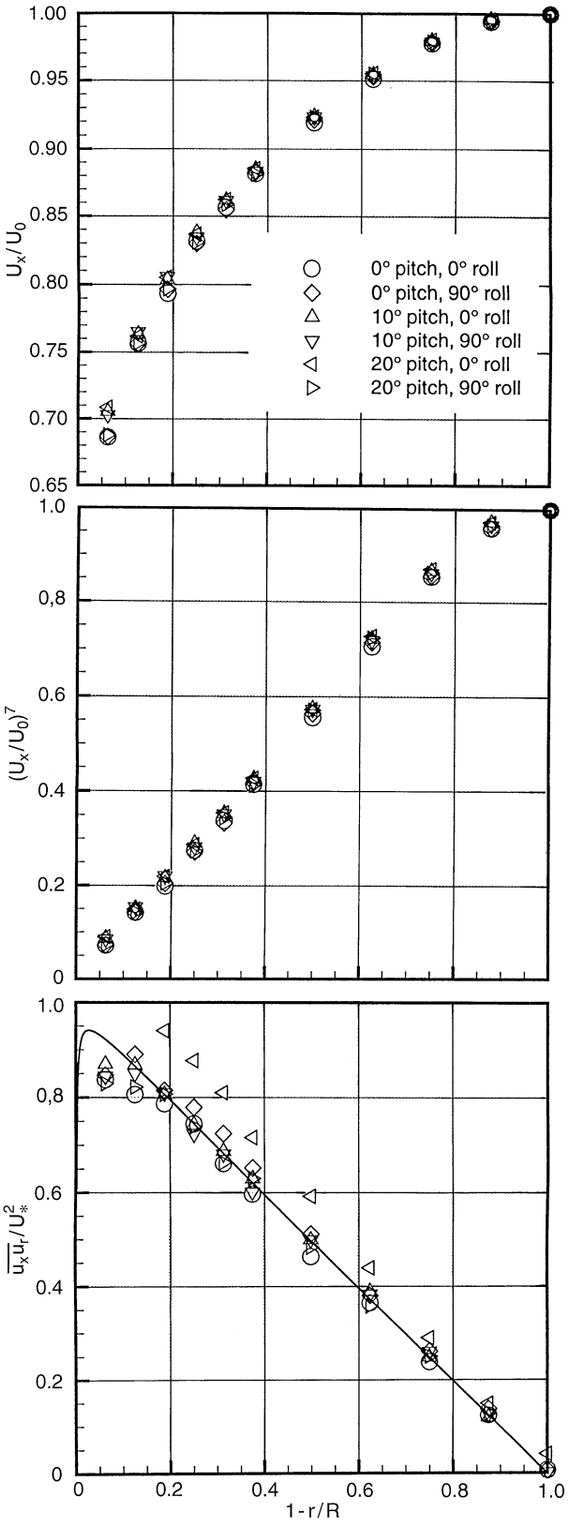

Fig. 7. Mean axial velocity and turbulent shear stress profiles measured in a fully developed pipe flow using the direct angle calibration technique. Legend lists probe angle with respect to pipe axis (location of mean flow within acceptance cone shown in Fig. 5). Solid line indicates theoretical profile

Measured velocity profiles are shown in Figs. 7 and 8. For all six probe orientations, the mean axial velocity profiles (Fig. 7) are very similar to each other and the $\frac{1}{7}$th-power law. The largest difference is only 2% U_∞ at $1-r/R=0.0625$ which could be due to the uncertainty in the probe position. Turbulent shear stress ($\overline{u_x u_r}$) profiles for the five probe orientations well inside the acceptance cone lie within $\pm 7\%$ of the theoretical profile for points as close to the wall as $1-r/R=0.125$. In fact, it is encouraging that the probe is measuring the shear stress to within 10% at $1-r/R=0.0625$ (about three measurement volumes away from the wall) considering the large axial velocity gradient. With the probe at 20° pitch, 0° roll, however, the measured turbulent shear stresses are approximately 17% high indicating some inaccuracy of the calibration or its interpolation at the limits of the acceptance cone. The axial turbulent normal stress ($\overline{u_x^2}$) profiles

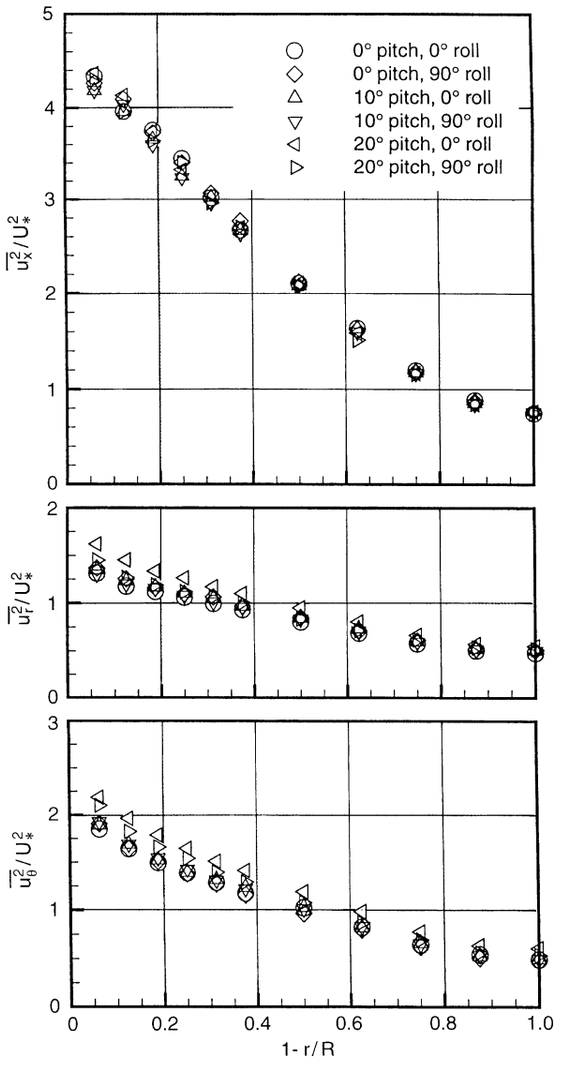

Fig. 8. Normal stress profiles measured in a fully developed pipe flow using the direct angle calibration technique. Legend lists probe angle with respect to pipe axis (location of mean flow within acceptance cone shown in Fig. 5)

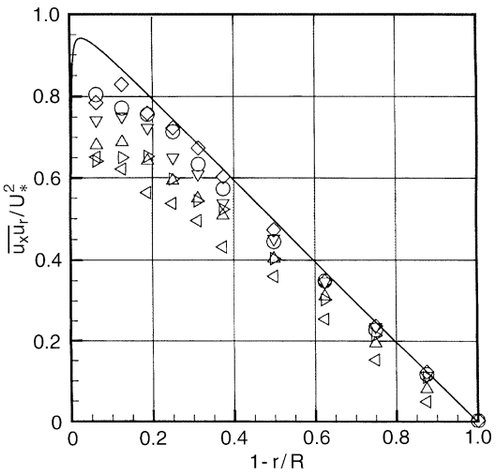

Fig. 9. Turbulent shear stress profiles measured in a fully developed pipe flow without using the direct angle calibration technique. Legend lists probe angle with respect to pipe axis

(Fig. 8) are within about 5% of each other for all probe orientations. The radial and tangential normal stresses measured for the 0 and 10° pitch orientations are almost identical. However, the profiles measured with the probe at 20° pitch vary from the others – up to 20% for the extreme case of 20° pitch, 0° roll, where the mean flow is close to the edge of the acceptance cone of the probe.

As an example of the importance of the direct angle calibration, Fig. 9 shows the $\overline{u_x u_r}$ profiles calculated using only the linearized equations (Eqs. (9)–(11)). As would be expected, increasing the misalignment between the probe axis and the mean flow, increases the error significantly. Also, these equations estimate non-zero values up to $23\% U_*^2$ for the $\overline{u_r u_\theta}$ and $\overline{u_x u_\theta}$ components.

Other, more circumstantial, evidence that this hot-wire system provides accurate measurements of turbulence stresses in a complex three-dimensional flow is contained in the work of Devenport et al. (1996). They measured in detail the turbulence stress field in the laminar vortex core of a tip vortex. Predictions of this stress field based upon the wandering motions of the vortex agreed very closely with the hot-wire data.

5 Conclusions

A velocity measurement system based on a miniature four-sensor hot-wire probe capable of simultaneous three-component measurements throughout a wide range of flow angles has been developed. The calibration technique allows measurements to be made throughout the acceptance cone of the probe without being restricted by the errors associated with analytic angle response equations. Calibration of the probe is accomplished in two parts: a velocity calibration which accounts for changing sensor properties, and an angle calibration which accounts for probe geometry. The angle calibration is a combination of analytic equations and look-up tables whose values tend to vary slowly allowing the use of a simple interpolation scheme. The formulation of the angle calibration makes clear the tradeoff between the complexity of the analytic model and the sophistication of the interpolation. The angle calibration is found to be nearly independent of velocity magnitude and cooling properties of the sensors. In principal, the calibration technique allows the probe to be used for measurements with up to a 30° angle between the probe axis and the flow direction. Measurements of turbulent shear and normal stresses in a fully developed pipe flow are accurate with the probe pitched up to 20°.

Appendix

The following is an analysis similar to that of Vukoslavčević and Wallace (1981), and Cutler and Bradshaw (1991), which was adapted to determine the significance of errors produced by velocity gradients for this particular four-sensor probe. Specifically, the errors resulting from use of Eqs. (9)–(11) where the velocity field is assumed constant across the measurement volume will be analyzed. This analysis therefore does not consider the look-up tables.

If the velocity field about a point located at the center of the measurement volume (U, V, W) is expanded as a first order Taylor series, the velocity field experienced by the center of the i-th sensor (U_i, V_i, W_i) is:

$$U_1 = U - \Delta_z \frac{\partial U}{\partial z}, \quad V_1 = V - \Delta_z \frac{\partial V}{\partial z}, \; W_1 = W - \Delta_z \frac{\partial W}{\partial z} \tag{16}$$

$$U_2 = U - \Delta_y \frac{\partial U}{\partial y}, \quad V_2 = V - \Delta_y \frac{\partial V}{\partial y}, \; W_2 = W - \Delta_y \frac{\partial W}{\partial y} \tag{17}$$

$$U_3 = U + \Delta_z \frac{\partial U}{\partial z}, \quad V_3 = V + \Delta_z \frac{\partial V}{\partial z}, \; W_3 = W + \Delta_z \frac{\partial W}{\partial z} \tag{18}$$

$$U_4 = U + \Delta_y \frac{\partial U}{\partial y}, \quad V_4 = V + \Delta_y \frac{\partial V}{\partial y}, \; W_4 = W + \Delta_y \frac{\partial W}{\partial y} \tag{19}$$

where $2\Delta_y$ is the distance between sensors 2 and 4, and $2\Delta_z$ is between sensors 1 and 3. Substituting Eqs. (16)–(19) into (5)–(8) and using the same assumptions used to obtain Eqs. (9)–(11), we find the errors due to the velocity gradients are:

$$U - U_e = \frac{\Delta_z \frac{\partial V}{\partial z}[\cos(\theta_1 - \theta_3) + \cos(\theta_1 + \theta_3)] - \Delta_z \frac{\partial U}{\partial z}\sin(\theta_3 - \theta_1)}{2\sin(\theta_1 + \theta_3)} + \frac{\Delta_y \frac{\partial W}{\partial y}[\cos(\theta_2 - \theta_4) + \cos(\theta_2 + \theta_4)] - \Delta_y \frac{\partial U}{\partial y}\sin(\theta_4 - \theta_2)}{2\sin(\theta_2 + \theta_4)} \tag{20}$$

$$V - V_e = \frac{\Delta_z \frac{\partial U}{\partial z}[\cos(\theta_1 - \theta_3) - \cos(\theta_1 + \theta_3)] + \Delta_z \frac{\partial V}{\partial z}\sin(\theta_3 - \theta_1)}{\sin(\theta_1 + \theta_3)} \tag{21}$$

$$W - W_e = \frac{\Delta_y \frac{\partial U}{\partial y}[\cos(\theta_2 - \theta_4) - \cos(\theta_2 + \theta_4)] + \Delta_y \frac{\partial W}{\partial y}\sin(\theta_4 - \theta_2)}{\sin(\theta_2 + \theta_4)} \tag{22}$$

For simplicity, consider the case of an ideal probe with $\theta_i = 45^\circ$, $\Delta_y = \Delta_z$. Equations (20)–(22) reduce to:

$$U - U_e = -\frac{1}{2}\Delta_y\left(\frac{\partial V}{\partial z} + \frac{\partial W}{\partial y}\right) \tag{23}$$

$$V - V_e = -\Delta_y \frac{\partial U}{\partial z} \tag{24}$$

$$W - W_e = -\Delta_y \frac{\partial U}{\partial y}. \tag{25}$$

These equations illustrate the basic relationships between the velocity errors and the local velocity gradients and are similar to those derived by Cutler and Bradshaw (1991). The averaging of the two U estimates results in the streamwise velocity gradient error (Eq. (23)) being proportional streamwise strain rate for the case of an ideal probe instead of the streamwise vorticity. This averaging can be essential in some situations (e.g. trailing vortex measurements).

References

Bearman PW (1971) Corrections for the effect of ambient temperature drift on hot-wire measurements in incompressible flow. DISA Inform 11: 25–30

Browne LBW; Antonia RA, Chua LP (1989) Calibration of X-Probes for turbulent flow measurement. Exp Fluids 7: 201–208

Cutler AD; Bradshaw P (1991) A crossed hot-wire technique for complex turbulent flows. Exp Fluids 12: 17–22

Devenport WJ; Glegg SAL; Sharma G (1992) Turbulence measurements in trailing vortices for B.W.I. noise prediction. Report to NASA Langely under grant NAG-1-1119

Devenport WJ; Rife MC; Liapis SI; Follin GJ (1996) The structure and development of a wing-tip vortex. J Fluid Mech 312: 67–106

Döbbeling K; Lenze B; Leuckel W (1990) Computer-aided calibration with a quadruple hotwire probe. Exp Fluids 8: 257–262

Jorgensen FE (1971) Directional sensitivity of wire and fibre-film probes. DISA Inform 11: 31–37

Kovasznay LSG (1954) Physical measurements in gas dynamics and combustion. 227, Princeton University Press

Leuptow RM; Breuer KS; Haritonidis JH (1988) Computer-aided calibration of X-probes using a look-up table. Exp Fluids 7: 201–208

Mathioudakis K; Breugelmans FAE (1985) Use of triple hot wires to measure unsteady flows with large direction changes. J Phy E: Sci Inst 18: 414–419

Nikuradse J (1932) Gesetzmässigkeit der turbulenten Strömung in glatten Rohren. VDI-Forschungsh 356 (Similarity for Turbulent Flow in Smooth Pipes)

Shaffer DM (1985) Reynolds stress measurement downstream of a turbine cascade. Master's thesis, VPI&SU, Blacksburg, VA

Vukoslavčević P; Wallace JM (1981) Influence of velocity gradients on measurements of velocity and steramwise vorticity with hot-wire X-array probes. Rev Sci Inst 52: 869–879